

From 2D to 1D in β -Naphthyne: A Porous Carbon Allotrope Merging Graphyne and Naphthylene

José A. S. Laranjeira^{a,*}, K. A. L. Lima^{b,c}, Nicolas F. Martins^a, Marcelo L. P. Junior^d, L.A. Ribeiro Junior^{b,c} and Julio R. Sambrano^a

^aModeling and Molecular Simulation Group, São Paulo State University (UNESP), School of Sciences, Bauru, 17033-360, SP, Brazil

^bInstitute of Physics, University of Brasília, Brasília, 70910-900, DF, Brazil

^cComputational Materials Laboratory, LCCMat, Institute of Physics, University of Brasília, Brasília, 70910-900, DF, Brazil

^dUniversity of Brasília, College of Technology, Department of Electrical Engineering, Brasília, 70910-900, DF, Brazil

ARTICLE INFO

Keywords:

Two-dimensional carbon allotrope
 β -naphthyne
Density functional theory
Mechanical anisotropy
1D structures

ABSTRACT

Two-dimensional (2D) carbon-based materials have attracted considerable interest due to their diverse structural and electronic properties, making them ideal for next-generation flat electronics. Among these materials, metallic-like porous structures offer advantages such as tunable charge transport and high surface area, which are essential for energy storage applications. In this study, we introduce β -naphthyne, a novel 2D carbon allotrope composed of naphthyl units interconnected by octagonal rings. First-principles calculations confirm its dynamic and thermal stability, demonstrating its theoretical feasibility. Our results confirm its energetic, dynamic, and mechanical stability and its metallic nature. Furthermore, we demonstrate that Young's modulus ranges from 46.60 N/m to 164.47 N/m, indicating an anisotropic mechanical response. Optical analysis reveals absorption activity in the infrared (IR) and ultraviolet (UV) regions. The 1D structures were also analyzed, revealing a Dirac cone and a transition from metallic to semiconducting behavior. These findings establish β -naphthyne as a promising material for energy storage and optoelectronic technologies.

1. Introduction

Two-dimensional (2D) carbon-based materials have garnered significant attention due to their mechanical, electronic, and optical properties, making them promising candidates for energy storage and nanoelectronics applications [1–3]. Among them, porous 2D carbon allotropes offer additional advantages while maintaining a high surface-to-volume ratio, exhibiting tunable electronic structures and enhanced ion diffusion, which are crucial for hydrogen storage, supercapacitors, and metal-ion batteries [4–9]. The incorporation of ordered nanopores into carbon frameworks can introduce novel electronic behaviors, such as Dirac cone semimetallicity, paving the way for the development of high-performance energy materials [9–11]. In this context, metallic-like porous 2D carbon allotropes can facilitate rapid charge transport while maintaining mechanical stability, essential properties for advanced energy storage applications.

Several porous carbon allotropes have been synthesized or theoretically predicted in recent years, each exhibiting distinct structural and electronic characteristics [4, 12–17]. For instance, graphdiyne, a synthesized material featuring acetylenic linkages, exhibits enhanced electrochemical performance due to its high charge carrier mobility and tunable bandgap [18]. Other experimentally synthesized materials include the biphenylene network, which was recently fabricated via on-surface synthesis and displays metallic behavior, holding potential for nanoelectronic applications [19]. In contrast, several computationally predicted structures [20–28] have been characterized, revealing distinct structural,

electronic, optical, and mechanical properties. However, the experimental realization of some of these structures remains a challenge [29]. Nevertheless, theoretical studies are essential for guiding experimental synthesis by predicting stability, mechanical response, and electronic characteristics, enabling researchers to design novel materials with desirable functionalities before fabrication [30, 31].

Building upon recent advances in 2D carbon-based materials for surface electronics, we introduce Naphthylene- β Graphyne (β -naphthyne) as a novel porous 2D carbon allotrope a novel porous 2D carbon allotrope characterized by naphthalene molecules covalently linked through acetylenic groups at all their dehydrogenated terminations, forming a rectangular symmetry. β -naphthyne is a graphyne-like version of β -naphthylene, previously proposed by Paz *et al.*, in which the allotrope is predicted from the naphthalene precursor in its so-called β phase, configuring a 2D carbon allotrope with 4-, 6-, and 10-membered rings [32]. In the structure proposed here, the linkage between naphthalene molecules is replaced by acetylenic groups, transforming the originally sp^2 -bonded system into a hybrid sp - sp^2 configuration, now exhibiting 6- and 8-membered rings, along with nanopores consisting of 18 carbon-membered units.

This structural design enhances electronic delocalization, offering a promising framework for energy storage applications. However, regarding the challenges of synthesizing such materials, naphthalene units no longer serve as a precursor for a potential synthesis of β -naphthyne. Instead, Octamethylnaphthalene ($C_{18}H_{24}$), synthesized in 1972 by Hart and Oku [33], emerges as a viable structural building

*Corresponding author
ORCID(s):

block for bottom-up synthesis strategies, such as surface-assisted polymerization or templated chemical vapor deposition (CVD), providing a feasible route for future syntheses of β -naphthyne [34–36].

This study presents the novel β -naphthyne structure, investigated through first-principles calculations. Using density functional theory (DFT), we explored its electronic properties, including band structures, electron localization functions (ELF), and Bader charge distribution. The thermal and dynamic stabilities were verified using *ab initio* molecular dynamics (AIMD) simulations. A comprehensive mechanical evaluation was conducted by analyzing elastic constants, with stability confirmed via the Born-Huang criteria. In addition, the effect of 1D confinement was evaluated by analysis of β -naphthyne nanoribbons. The findings reported here not only highlight the β -naphthyne as a 2D reliable carbon allotrope but also suggest its potential as a platform for diverse applications, such as energy storage, gas detection, and electronics.

2. Methodology

To explore the structural, electronic, mechanical, and optical properties of β -naphthyne, we conducted first-principles simulations based on DFT [37]. The computational framework was implemented using the Vienna Ab Initio Simulation Package (VASP) [38]. For electron exchange and correlation effects, we employed the generalized gradient approximation (GGA) following the Perdew-Burke-Ernzerhof (PBE) functional [39]. The interaction between valence and core electrons was treated using the projector-augmented wave (PAW) method [40], which enhances computational efficiency while preserving high precision.

The kinetic energy cutoff for the plane-wave basis set was set to 520 eV, ensuring an accurate representation of electronic states. The structural optimizations were performed using the conjugate gradient method until the force on each atom was lower than 0.01 eV/Å, and the total energy change between successive steps was below 10^{-5} eV. A vacuum spacing of 15 Å along the out-of-plane direction was introduced to prevent interactions between periodic images. The Brillouin zone was sampled using a Γ -centered Monkhorst-Pack \mathbf{k} -point mesh of $3 \times 3 \times 1$ ($18 \times 18 \times 1$) for monolayers and $3 \times 1 \times 1$ ($18 \times 1 \times 1$) for nanoribbons for optimization (density of states) calculations. Dispersion interactions were included using Grimme's DFT-D2 method [41], accounting for van der Waals forces to accurately describe interatomic interactions in porous carbon frameworks.

To evaluate the dynamical stability of β -naphthyne, phonon dispersion calculations were performed using density functional perturbation theory (DFPT) as implemented in the Phonopy package [42]. Additionally, *ab initio* molecular dynamics (AIMD) simulations were conducted at 300 K for 5 ps in the NVT ensemble, employing the Nosé-Hoover thermostat [43, 44] to assess its thermal robustness.

Electronic properties were examined through band structure and density of states calculations. The band structure was computed along high-symmetry paths of the Brillouin

zone to reveal Dirac cone features. At the same time, the projected density of states was used to analyze orbital contributions to electronic states. The first-order resonant Raman spectra at various laser energies were also estimated.

The optical properties were investigated through calculations of the frequency-dependent dielectric function, from which absorption coefficients and reflectance spectra were derived [45], providing insight into the potential optoelectronic applications of β -naphthyne.

The thermodynamic stability of β -naphthyne was analyzed by its cohesive energy (E_{coh}):

$$E_{\text{coh}} = \frac{E_{\beta\text{-naphthyne}} - \sum_i n_i E_i}{\sum_i n_i}, \quad (1)$$

where $E_{\beta\text{-naphthyne}}$ is the total energy of the structure, E_i represents the energy of isolated C atoms, and n_i is the atom count of each element. The same approach was used to obtain the E_{coh} for other 2D structures discussed in this work.

To analyze the vibrational properties of β -naphthyne, the coupled perturbed HF/Kohn–Sham algorithm [46] implemented in the computational package CRYSTAL17 [47] was used. The calculations in CRYSTAL17 were performed using triple-zeta valence with polarization (TZVP) basis set [48] together with the B3LYP functional. The structure was optimized by checking the root mean square (RMS) and the absolute value of the largest component of both the gradients and the estimated displacements. The convergence criteria used in the optimization for RMS and the largest component for gradient (0.00030 a.u. and 0.00045 a.u.) and displacement (0.00120 a.u. and 0.00180 a.u.), respectively. The reciprocal space was sampled using Pack-Monkhost and Gilat nets with sublattice and a shrinking factor of 12.

3. Results

3.1. Structure and Stability

β -naphthyne is characterized by a rectangular conventional unit cell that belongs to the Cmm (no. 65) space group, with lattice parameters $a = 10.74$ Å and $b = 11.72$ Å (see Fig. 1). The primitive cell comprises lattice parameters $a = b = 7.82$ Å, $\alpha = \beta = 90^\circ$, and $\gamma = 93.17^\circ$. The conventional unit cell consists of five crystallographically distinct carbon atoms located in C1 (0.764, 0.378, 0.500), C2 (0.359, 0.181, 0.500), C3 (0.566, 0.282, 0.500), C4 (0.367, 0.392, 0.500), and C5 (0.932, 0.000, 0.500). This structure forms a 2D carbon framework comprising 6–8 carbon-membered rings, where octagonal rings interconnect naphthyl fragments. For comparison purposes, Table 1 details the lattice parameters (a , b , $\alpha = \beta$, and γ), space group (SPG), band gap energy (E_{gap}), and cohesive energy (E_{coh}) for several carbon monolayers. The comparison shows that the cohesive energy (E_{coh}) of β -naphthyne (-7.25 eV/atom) is competitive with other 2D carbon allotropes, being close to that of T-graphene (-7.45 eV/atom) and graphenylene

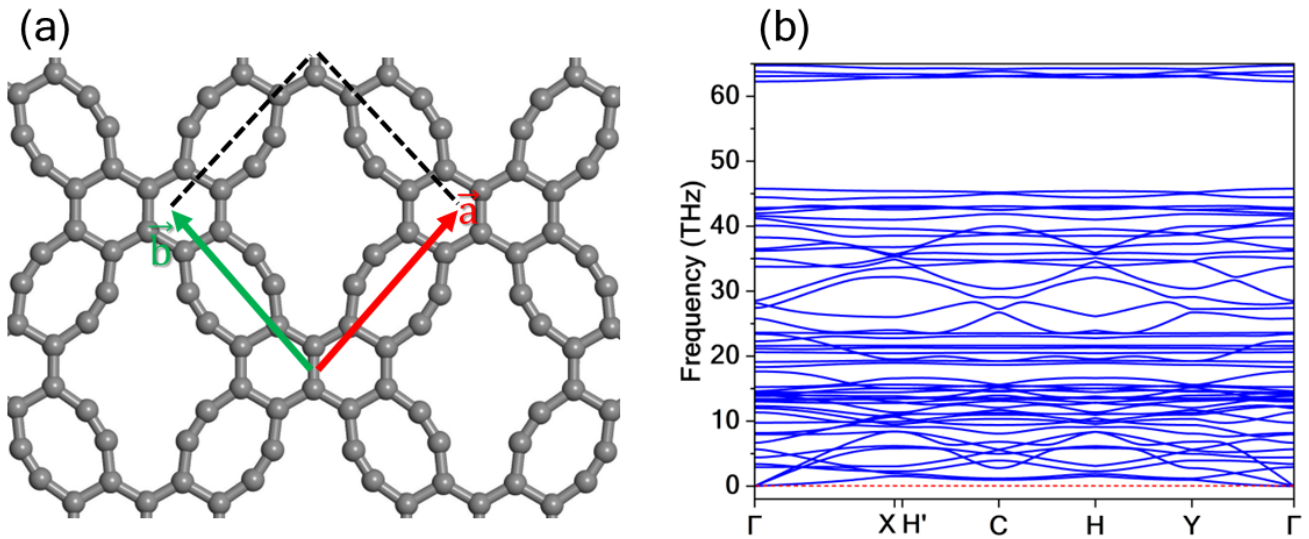


Figure 1: (a) Top view of the optimized atomic structure of β -naphthyne. The unit cell has primitive lattice vectors $a = b = 7.82$ Å. (b) Phonon dispersion spectrum of β -naphthyne along high-symmetry paths of the Brillouin zone.

Table 1

Lattice parameters (a and b in Å, $\alpha = \beta$, and γ in degrees), space group (SPG), band gap energy (E_{gap}) in eV, and cohesive energy (E_{coh}) in eV/atom obtained for Holey-graphenylene and other relevant 2D carbon allotropes at DFT/GGA-PBE level. The values reported in this table were calculated in this study.

	a	b	$\alpha = \beta$	γ	SPG	E_{gap}	E_{coh}
β -naphthyne (this work)	10.74	11.43	90	90	Cmm (65)	Metallic	-7.25
T-graphene [49]	3.45	3.45	90	90	$P4/mmm$ (123)	Metallic	-7.45
Twin-graphene [50]	6.14	6.14	90	120	$P6/mmm$ (191)	0.73	-7.08
PHE-graphene [51]	5.73	5.73	90	120	$P6m2$ (187)	Metallic	-7.56
Penta-graphene [21]	3.64	3.64	90	90	$P42_1m$ (113)	2.19	-7.13
Graphyne [52]	9.46	9.46	90	120	$P6/mmm$ (191)	Metallic	-7.20
Graphenyldiene [28]	6.07	6.07	90	90	$P4/mbm$ (127)	0.78	-6.92
Graphenylene [27, 53]	6.77	6.77	90	120	$P6/mmm$ (191)	0.04	-7.33
Biphenylene [19]	3.80	4.50	90	90	$Pmmm$ (47)	Metallic	-7.47
Graphene [54]	2.47	2.47	90	120	$P6/mmm$ (191)	Metallic	-8.02

(-7.33 eV/atom), but lower than that of pure graphene (-8.02 eV/atom). The E_{coh} reflects the energy required to disassemble a solid into isolated atoms, serving as a key indicator of the structural stability of the material. Therefore, while β -naphthyne shows slightly weaker cohesion than graphene, its value remains sufficiently high to imply a stable 2D structure.

To evaluate the dynamical stability of β -naphthyne, the phonon band dispersion was computed along the high-symmetry paths of the Brillouin zone, as depicted in Fig. 1(b). The phonon spectrum confirms the absence of imaginary frequencies, indicating that the material is dynamically stable. At the Γ -point, the phonon dispersion exhibits three acoustic modes with a characteristic linear behavior. Several phonon branches remain relatively flat in the 18–25 THz range, suggesting low group velocity and localized vibrational modes. In contrast, the bands display quadratic dispersion in the 25–35 THz range, indicating high phononic mobility. Finally, vibrational modes with flat characteristics

above 60 THz correspond to the sp-hybridized bonds in β -naphthyne, a common feature in graphyne-like systems [55].

One critical aspect in assessing the viability of novel 2D materials is their thermal stability under ambient conditions. In this way, AIMD simulations were performed at 300 K for a total duration time of 4 ps. Fig. 2(a) depicts the evolution of the total energy fluctuations during the simulation, along with the final atomic configuration (Fig. 2(b)).

Fig. 2(a) shows the total energy as a function of time, with an initial stabilization period within the first picosecond of the simulation. After this phase, energy fluctuations remain minimal, consistently within a range of less than 1 eV, indicating structural robustness. The absence of significant deviations suggests that no phase transitions or reconstruction events occur during the simulation, further supporting the stability of the material at room temperature. The final atomic configuration, presented in Fig. 2(b), further corroborates this observation. The top and side views reveal that the structural integrity of β -naphthyne is preserved, with only minor out-of-plane distortions emerging.

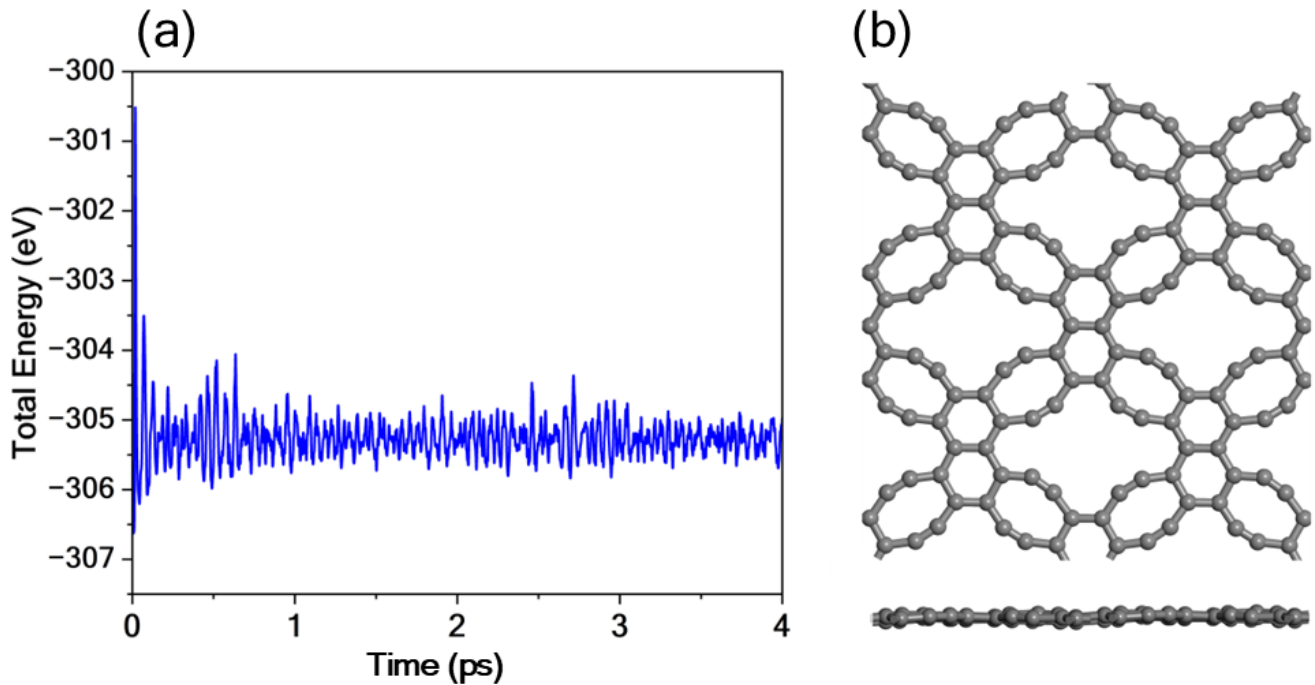


Figure 2: (a) Evolution of total energy as a function of time obtained at 300 K over 4 ps. (b) Final atomic configuration after the AIMD run, showing top and side views of the structure.

3.2. Electronic Analysis

We performed a detailed analysis of the band structure to investigate the electronic properties of β -naphthyne. The results, depicted in Fig. 3, confirm that β -naphthyne exhibits metallic behavior with a band partially occupied crossing the Fermi level (E_F) closer to the Γ point. The states that compose this band can act as acceptor states, receiving the electronic density and opening the material band gap. This can be useful for an effective interaction with metal adatoms. In the valence band (VB), one can note that the bands display high dispersion, with several crossings, revealing a strong coupling between the electronic states. On the other hand, when the conduction band (CB) is analyzed, the lowest energy band touches E_F two times at the points H' and H . This band presents a high dispersion, around 2 eV.

The projected density of states (PDOS) analysis provides a more detailed understanding of the electronic structure, shown in Fig. 4, which decomposes the total density of states into atomic orbital contributions. The valence and conduction bands predominantly comprise p orbitals, with the p_y states contributing most significantly, closely followed by the p_x states. The similar energy distribution profiles of the p_y and p_x orbitals suggest a strong orbital coupling in these energy regions. However, near the Fermi level, it becomes evident that only the p_z orbitals contribute, indicating a pronounced π -character in this energy range.

To further investigate the electronic properties of β -naphthyne, we analyzed the spatial distribution of its frontier molecular orbitals, specifically the highest occupied crystalline orbital (HOCO) and the lowest unoccupied crystalline orbital (LUCO), as shown in Fig. 5. Fig. 5(a) illustrates

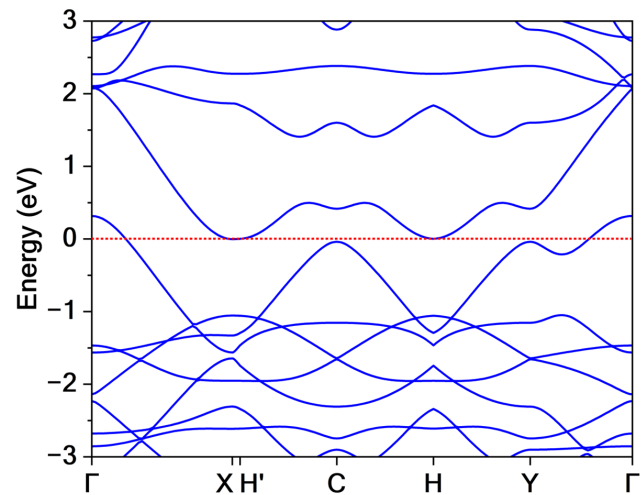


Figure 3: The electronic band structure of β -naphthyne is depicted along the high-symmetry trajectories within the Brillouin zone. For clarity, the Fermi level is indicated by the red dashed line.

the HOCO, which is predominantly composed of π -type orbitals localized on the naphthyl units. The electron density is highly delocalized across the hexagonal rings, indicating a strong conjugation network that enhances hole mobility. The side view further confirms the planarity of the electronic distribution, reinforcing the 2D nature of the conduction pathways.

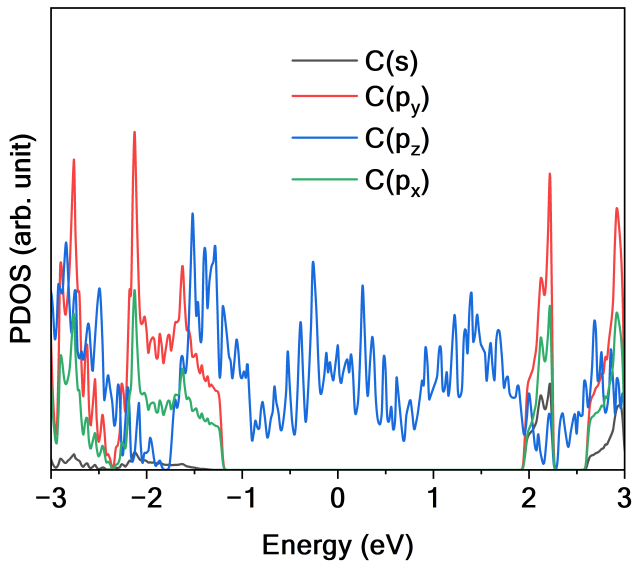


Figure 4: Projected density of states (PDOS) of β -naphthyne, showing the orbital-resolved contributions to the electronic structure.

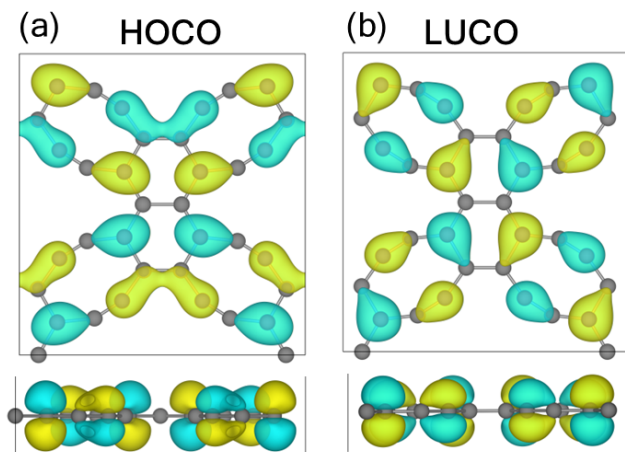


Figure 5: (a) Spatial distribution of the highest occupied crystalline orbital (HOCO) and (b) the lowest unoccupied crystalline orbital (LUCO) of β -naphthyne.

Fig. 5(b) shows the LUCO, which also exhibits a π -character, but with electron density more prominently localized around the octagonal rings. This spatial separation between the HOCO and LUCO suggests a moderate charge transfer character, which could influence optical excitations and recombination rates. The LUCO distribution indicates that electron transport might be primarily facilitated through the octagonal framework, complementing the hole conduction pathways of the HOCO.

The distinct spatial location of HOCO and LUCO further supports the metallic nature of β -naphthyne, as both orbitals maintain a significant density near the Fermi level. The overlap of these orbitals could also contribute to strong

optical absorption, suggesting potential applications in photodetectors and optoelectronic devices, as will be discussed later.

To gain a deeper understanding of the charge distribution and bonding nature of β -naphthyne, we analyzed its electron localization function (ELF), as shown in Fig. 6. The ELF provides valuable information on the degree of electron localization, where a value of 1 indicates strongly localized electrons (e.g., covalent bonds or lone pairs), a value of 0.5 corresponds to a homogeneous electron gas-like distribution, and a value of 0 represents regions with minimal or no electron density.

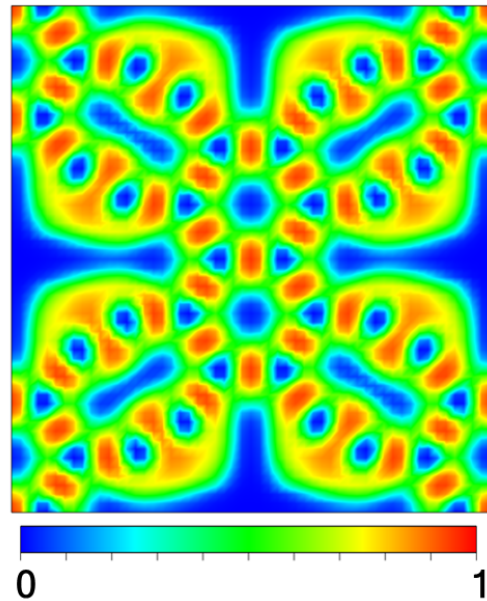


Figure 6: Electron Localization Function (ELF) of β -naphthyne.

In β -naphthyne, the naphthyl fragments exhibit high ELF values, consistent with the resonant nature of benzene rings, where delocalized π -electrons contribute to moderately high electron localization due to sp^2 hybridization. In contrast, the octagonal rings exhibit lower ELF values, indicating greater electron delocalization than the naphthyl units. This behavior can be attributed to sp -hybridized bonds, which result in a more diffuse electron density along the in-plane bonds. The lower ELF in these regions suggests that the electronic structure of the octagonal motifs contributes to anisotropic charge transport, complementing the conduction pathways of the naphthyl fragments.

The ELF map further supports the conclusion that β -naphthyne exhibits a highly delocalized electronic structure, with distinct regions contributing to different transport properties. The hybridized bonding interactions within the naphthyl and octagonal rings create a unique electronic environment, making this material a promising candidate for nanoelectronic and optoelectronic applications, where controlled charge delocalization and transport are essential.

3.3. Optical Properties

To address the optical properties of β -naphthyne, we calculated its absorption coefficient (α) and reflectance (R), as illustrated in Fig. 7. The visible light range is highlighted in the figure to facilitate the identification of its transparency and absorption characteristics.

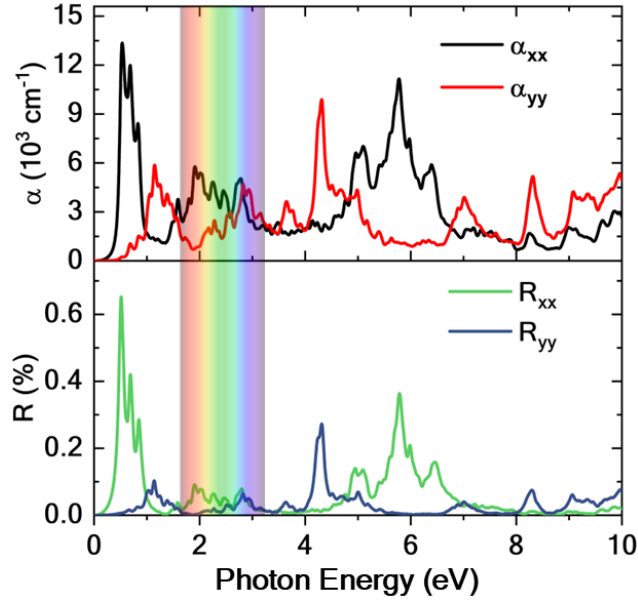


Figure 7: Optical properties of β -naphthyne. (Top panel) Absorption coefficient (α) as a function of photon energy for the x (black) and y (red) polarization components. (Bottom panel) Reflectance (R) for the x (green) and y (blue) components.

β -naphthyne exhibits strong absorption in the IR region, where the absorption coefficient reaches approximately $14 \times 10^3 \text{ cm}^{-1}$ for the x component. This result suggests that the material could be well-suited for IR photodetectors and thermal shielding applications. Additionally, the y component shows noticeable absorption in the near-IR range, further reinforcing its potential use in IR-active optoelectronic devices.

The material displays relatively low absorption in the visible spectrum, with the maximum absorption coefficient reaching $6 \times 10^3 \text{ cm}^{-1}$ between the red and orange spectral regions for the x component. This trend indicates that β -naphthyne is mainly transparent to visible light, making it a promising candidate for transparent conducting films or low-energy-loss optical coatings. The reflectance in this range remains minimal, further confirming that the material has low optical reflection and high light transmission properties. β -naphthyne exhibits strong absorption peaks in the UV region, with significant transitions occurring around 4.5 eV (y component) and 6 eV (x component). These absorption peaks are accompanied by increased reflectance, indicating that the material effectively interacts with high-energy photons in this range.

3.4. Vibrational Properties

Vibrational spectroscopy provides essential insights into the bonding nature and structural integrity of materials. To assess the phonon behavior of β -naphthyne, we computed both the Raman and IR spectra, as shown in Fig. 8. These spectra allow us to distinguish between Raman-active and IR-active vibrational modes, shedding light on the symmetry and electronic environment of atomic vibrations in the material.

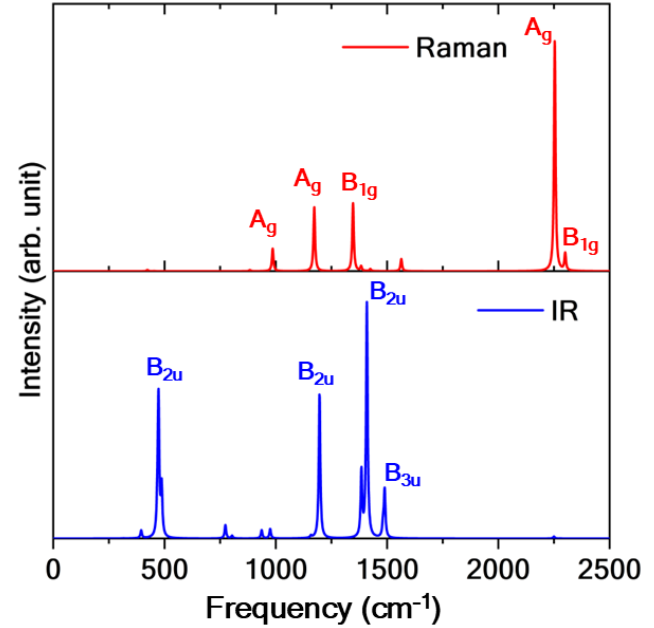


Figure 8: (Top/Bottom panel) Raman/Infrared spectrum of β -naphthyne.

To obtain Raman and IR spectra (Fig. 8), the CPHF/KS approach implemented in CRYSTAL17 was utilized. The vibration modes of holey-naphthylene can be represented by $\Gamma_{vib} = 5B_{1u} + 9B_{2u} + 9B_{3u} + 4B_{2g} + 4A_u + 5B_{3g} + 9B_{1g} + 9A_g$. Between these modes, three are acoustic ($B_{1u} + B_{2u} + B_{3u}$), four are silent ($4A_u$), 23 are IR-active ($5B_{1u} + 9B_{2u} + 9B_{3u}$), and 27 are Raman-active ($4B_{2g} + 5B_{3g} + 9B_{1g} + 9A_g$).

Analyzing the Raman spectrum (Fig. 8, top panel) reveals several distinct peaks, with the most intense modes A_g and B_{1g} occurring at low and intermediate frequencies. Four prominent bands are visible at 985 cm^{-1} (A_g), 1172 cm^{-1} (A_g), 1383 cm^{-1} (B_{1g}), and 2253 cm^{-1} (A_g). Strong A_g symmetric modes suggest collective in-plane stretching and breathing vibrations of the carbon framework. The sharp intensity of these peaks highlights the high rigidity of the system, which is commonly observed in sp^2 -hybridized carbon networks. The prominent peak at the high-frequency region corresponds to a strong C–C stretching mode, a signature of a well-preserved conjugated structure in the material.

However, by verifying the IR spectrum (Fig. 8, bottom panel), several intense peaks associated with asymmetric

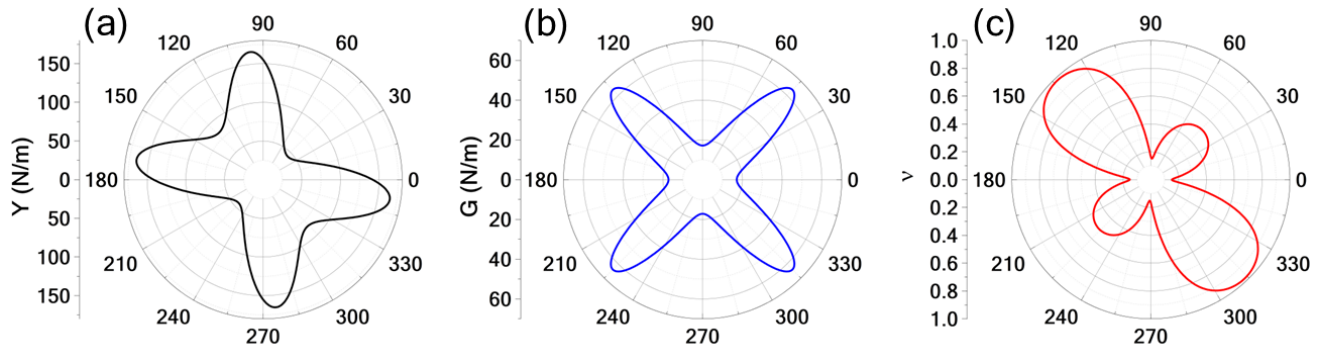


Figure 9: Polar plots of (a) Young's modulus (Y), (b) Shear modulus (G), and (c) Poisson's ratio (ν).

for β -naphthylene, demonstrating their mechanical anisotropy.

stretching and bending modes are shown. Four intense bands are noticed at 472 cm^{-1} (B_{2u}), 1196 cm^{-1} (B_{2u}), 1409 cm^{-1} (B_{2u}), and 1489 cm^{-1} (B_{3u}) are observed. The B_{2u} and B_{3u} indicate dipole-active vibrations arising from charge asymmetry within the structure. The strongest IR peak, located around 1500 cm^{-1} , is related to C–C stretching motions similar to those observed in other 2D carbon-based materials [56, 57]. The presence of multiple low-frequency peaks suggests the existence of out-of-plane bending and deformation modes, which contribute to the dynamic flexibility of the monolayer.

3.5. Mechanical Properties

The mechanical properties of β -naphthylene were assessed by calculating its elastic constants, which are crucial to determining the material's structural stability and mechanical response. The obtained values for the independent elastic constants are $C_{11} = 169.10\text{ N/m}$, $C_{22} = 173.64\text{ N/m}$, $C_{12} = 42.68\text{ N/m}$, $C_{16} = -22.32\text{ N/m}$, $C_{26} = -17.49\text{ N/m}$, and $C_{66} = 20.98\text{ N/m}$. According to the Born-Huang stability criteria [58], the mechanical stability of 2D oblique systems is ensured if $C_{11} > 0$, $C_{11}C_{22} > C_{12}^2$, and $\det(C_{ij}) > 0$. Substituting the calculated values, these conditions are all satisfied. Therefore, we confirm that the β -naphthylene structure is mechanically stable under small deformations.

One can note that Young's modulus (Y), which quantifies the material's resistance to uniaxial deformation, exhibits strong anisotropy. As shown in Fig. 9(a), Y reaches a maximum of 165.88 N/m along one crystallographic direction and a minimum of 43.71 N/m in the perpendicular direction, resulting in an anisotropy ratio of 3.79. This trend indicates that the material's stiffness strongly depends on the applied strain direction. The maximum Young's modulus of β -naphthylene surpasses that of graphenyldiene (122.47 N/m) and graphyne (123.59 N/m) (refer to Table 2), reinforcing its classification as a graphyne-like monolayer due to the presence of sp-bonded carbon atoms.

The shear modulus (G), which describes the resistance to shear deformations, also demonstrates notable directional variation. Fig. 9(b) depicts that G varies from 63.93 N/m to 17.17 N/m , corresponding to an anisotropy ratio of 3.73.

Interestingly, the maximum shear modulus exceeds that of graphenyldiene (45.29 N/m) and graphyne (42.63 N/m), suggesting that β -naphthylene resists shear forces more effectively than other related 2D carbon materials. The Poisson's ratio (ν), shown in Fig. 9(c), exhibits the highest degree of anisotropy, ranging from 0.98 to 0.15, with an anisotropy ratio of 6.48. This extreme variation indicates that β -naphthylene's ability to contract in one direction when stretched in another highly depends on the strain orientation. Interestingly, the material can mimic Poisson's graphene ratio, which is considered one of the most mechanically robust materials. The pronounced mechanical anisotropy of β -naphthylene is among the highest reported for 2D carbon allotropes, even exceeding that of T-graphene, which was previously considered one of the most anisotropic 2D materials.

3.6. One-dimensional (1D) structures

We now turn our attention to nanoribbons derived from β -naphthylene. Due to their rectangular lattice, the nanoribbons were generated by exploring the cutting directions of the armchair (y or b) and zigzag (x or a). The armchair and zigzag β -naphthylene nanoribbons are referred to as ANNRR and ZNNR, respectively. For ZNNR, we considered a single type of edge in the nonperiodic direction, consisting of two hexagons, as illustrated in Fig. 10a. In the case of ANNRRs, two edge terminations were examined: one with two hexagons (hh) (Fig. 10b) and another with a single hexagon (h) (Fig. 10c), labeled ANNRR- hh and ANNRR- h , respectively. The chosen nanoribbon width spans three naphthyl groups. This methodology is in agreement with the approach adopted by Paz et al. [32] in their investigation of the 1D structures of β -naphthylene. Note that β -naphthylene nanoribbons did not show reconstructions or bond breaks in optimization. In addition, the planarity of 2D β -naphthylene was maintained.

To explore the electronic properties of the β -naphthylene 1D structures, we calculated the band structures for ZNNR, ANNRR- h , and ANNRR- hh , as depicted in Fig. 11. The ZNNR retains a metallic character, mirroring its 2D counterpart. However, a remarkable characteristic emerges with a Dirac

Table 2

Maximum and minimum values of Young's modulus (Y_{\max} , Y_{\min}) (N/m), Poisson ratio (ν_{\max} , ν_{\min}), and Shear modulus (G_{\max} , G_{\min}) (N/m) for α , β , and γ -anthraphenylenes and other carbon monolayers. The values reported in this table were calculated in this study.

	Y_{\max}/Y_{\min}	ν_{\max}/ν_{\min}	G_{\max}/G_{\min}
β -naphthyne	165.88/43.71	0.98/0.15	63.94/17.17
PHE-graphene	262.29/262.29	0.26/0.26	103.91/103.91
Graphenylene	209.02/209.02	0.27/0.27	82.11/82.11
Graphene	345.42/345.42	0.17/0.17	147.60/147.60
Graphenyldiene	122.47/122.47	0.35/0.35	45.29/45.29
Penta-graphene	271.81/266.67	-0.08/-0.10	151.21/144.98
T-graphene	293.90/148.02	0.16/0.58	126.57/148.02
Graphyne	123.59/123.59	0.45/0.45	42.63/42.63

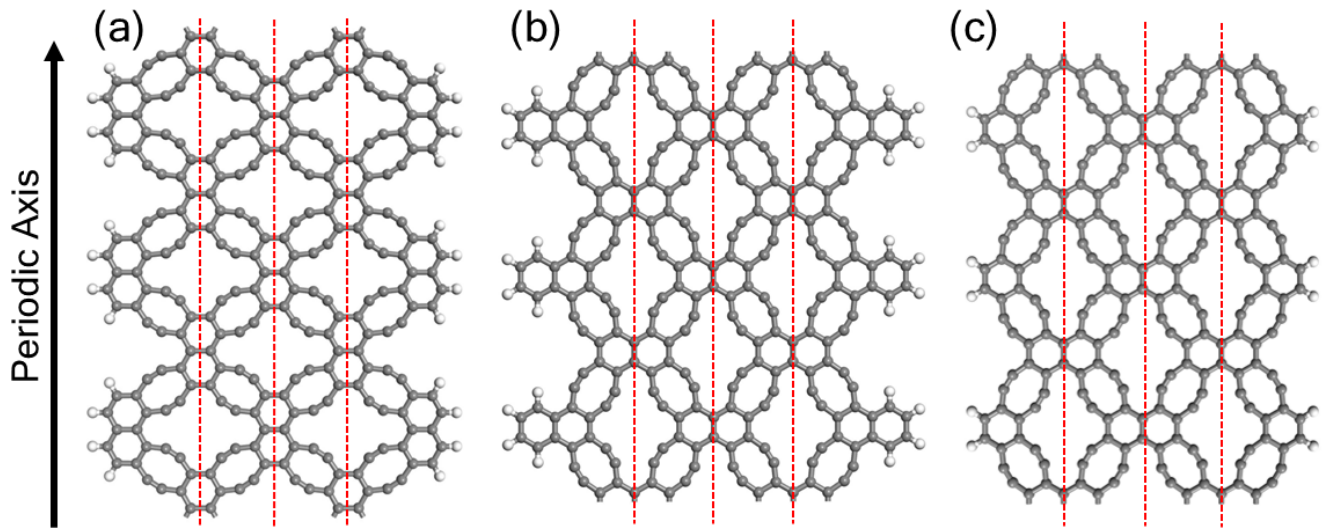


Figure 10: Schematic representation of the 1D structures of β -naphthyne nanoribbons. (a) Zigzag nanoribbon (ZNNR), (b) armchair nanoribbon with double hexagon edges (ANNR- hh), and (c) armchair nanoribbon with single hexagon edges (ANNR- h).

cone positioned closer to the Γ point. In contrast, the ANN- hh and ANN- h structures reveal a transition from metallic to semiconducting behavior, with direct band gaps at the Γ point of 0.08 eV and 0.24 eV, respectively. This band gap opening can be attributed to the edge-induced symmetry-breaking and quantum confinement effects inherent to the reduced dimensionality.

To verify the composition of the electronic states of the β -naphthyne nanoribbons, the projected density of states (PDOS) was calculated, as shown in Fig. 12. The general features closely resemble those of the 2D counterpart, such as the prominent contribution of p_y and p_x states at the lower and higher energies of the valence band (VB) and conduction band (CB), respectively. Around the Fermi level (E_F), the p_z states dominate entirely, with no significant contributions from other orbitals. Furthermore, hydrogen states do not show relevant influence across the evaluated energy range.

For ZNNR (Fig. 12(a)), despite the presence of a Dirac cone, the PDOS reveals a non-zero density of states at the Fermi level. This finite DOS arises from the low dispersion of bands near the Dirac point, causing an accumulation of electronic states around E_F , preventing the DOS from

vanishing completely. In the cases of ANN- hh (Fig. 12(b)) and ANN- h (Fig. 12(c)), a noticeable accumulation of states at the band edges is observed, accompanied by an abrupt drop in the DOS at these regions, characteristic of highly correlated electronic states.

4. Conclusion

In this work, we explore the structural, electronic, mechanical and optical properties of a novel porous 2D carbon allotrope, β -naphthyne, using first-principles calculations. Our results confirmed its stability, with phonon dispersion and AIMD simulations indicating a robust framework.

The electronic band structure revealed that β -naphthyne exhibits metallic behavior, with strong π -character for the states in the band edges. Mechanical analysis highlighted its strong anisotropy, showing a significant directional dependence on Young's modulus, shear modulus, and Poisson's ratio. This mechanical anisotropy surpasses that of previously studied 2D carbon materials, positioning β -naphthyne as a promising candidate for strain engineering applications.

Optical investigations demonstrated that β -naphthyne exhibits strong IR absorption, moderate interaction within

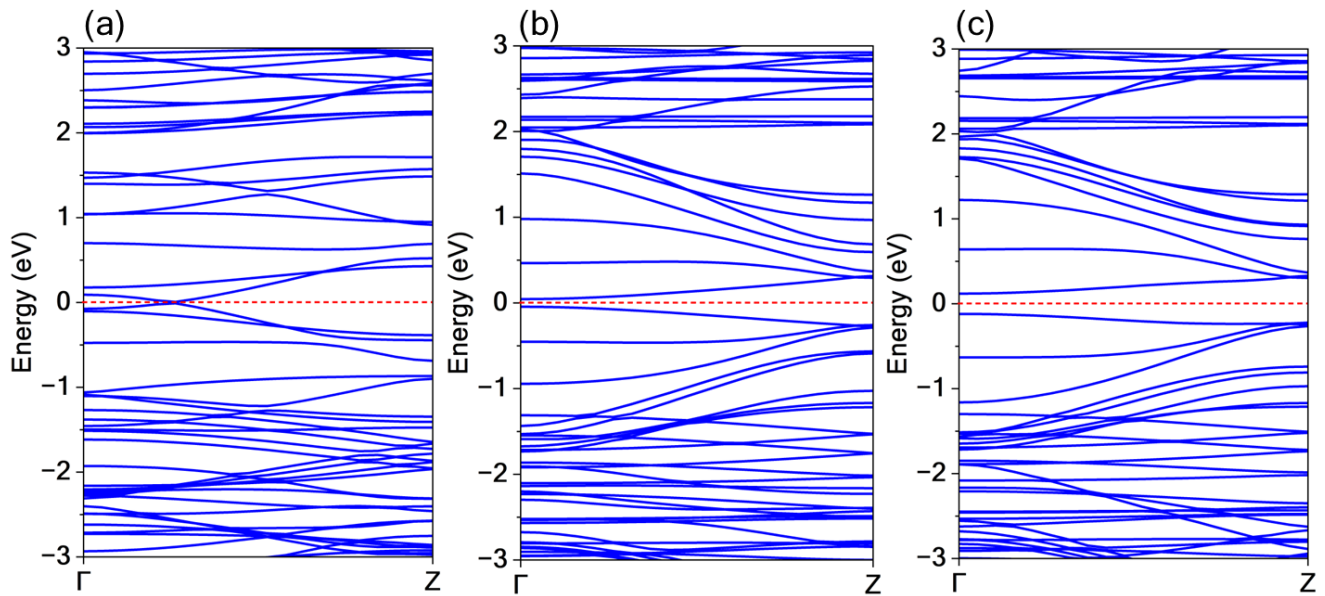


Figure 11: The electronic band structure of β -naphthylene 1D structures for (a) ZNNR, (b) ANNR-*hh*, and ANNR-*h*. The red dashed line indicates the Fermi level.

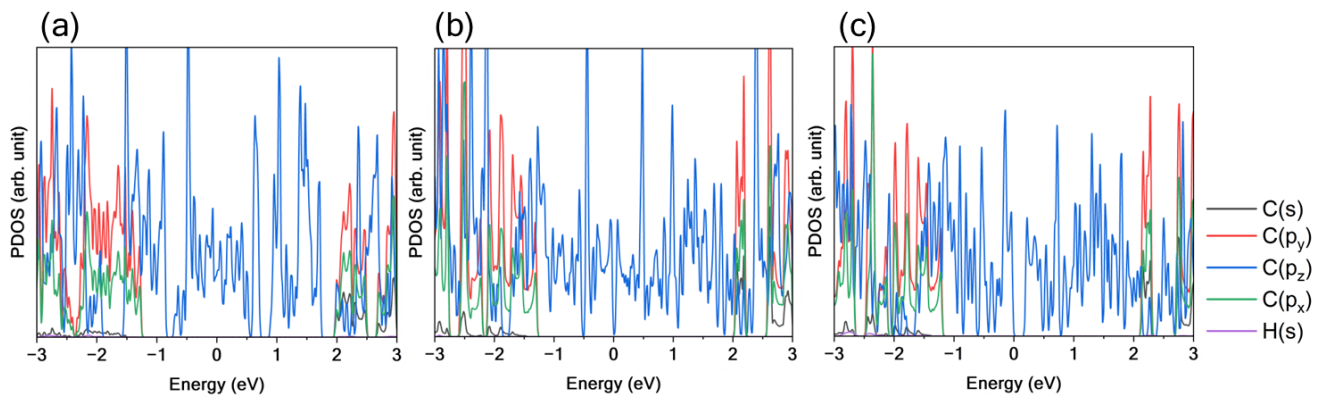


Figure 12: Projected density of states (PDOS) of β -naphthylene 1D structures for (a) ZNNR, (b) ANNR-*hh*, and ANNR-*h*.

the visible spectrum, and pronounced UV absorption peaks, suggesting its potential for optoelectronic and photonic technologies. Furthermore, the Raman and IR spectra provided distinctive vibrational fingerprints, providing a reliable reference for future experimental validation.

We further examine the electronic properties of 1D β -naphthylene nanoribbons. Although ZNNR retained the metallic character of its 2D counterpart, ANNR-*h* and ANNR-*hh* showed a transition from metallic to semi-conducting behavior, with direct band gaps of 0.08 and 0.24 eV, respectively. These findings underscore the tunable electronic properties of β -naphthylene, driven by dimensionality reduction and edge geometry, broadening its potential for nanoelectronic applications.

Data access statement

Data supporting the results can be accessed by contacting the corresponding author.

Conflicts of interest

The authors declare no conflict of interest.

Acknowledgements

This work was supported by the Brazilian funding agencies Fundação de Amparo à Pesquisa do Estado de São Paulo - FAPESP (grant no. 2022/03959-6, 2022/14576-0, 2020/01144-0, 2024/05087-1, and 2022/16509-9), and National Council for Scientific, Technological Development - CNPq (grant no. 307213/2021-8). L.A.R.J. acknowledges the financial support from FAP-DF grants 00193.00001808/2022-71 and 00193 - 00001857/2023 - 95, FAPDF-PRONEM grant 00193.00001247/2021-20, PDPG-FAPDF-CAPES Centro-Oeste 00193-00000867/2024-94, and CNPq grants 350176/2022-1 and 167745/2023 - 9.

CRedit authorship contribution statement

José A. S. Laranjeira: Conceptualization of this study, Methodology, Review and editing, Investigation, Formal analysis, Writing – review & editing, Writing – original draft. **K. A. L. Lima:** Conceptualization of this study, Methodology, Review and editing, Investigation, Formal analysis, Writing – review & editing, Writing – original draft. **Nicolas F. Martins:** Conceptualization of this study, Methodology, Review and editing, Investigation, Formal analysis, Writing – review & editing, Writing – original draft. **Marcelo L. P. Junior:** Conceptualization of this study, Methodology, Review and editing, Investigation, Formal analysis, Writing – review & editing, Writing – original draft. **L.A. Ribeiro Junior:** Conceptualization of this study, Methodology, Review and editing, Investigation, Formal analysis, Writing – review & editing, Writing – original draft. **Julio R. Sambrano:** Conceptualization of this study, Methodology, Review and editing, Investigation, Formal analysis, Writing – review & editing, Writing – original draft.

References

- [1] Santosh K Tiwari, Vijay Kumar, Andrzej Huczko, R Oraon, A De Adhikari, and GC Nayak. Magical allotropes of carbon: prospects and applications. *Critical Reviews in Solid State and Materials Sciences*, 41(4):257–317, 2016.
- [2] Salisu Nasir, Mohd Zobir Hussein, Zulkarnain Zainal, and Nor Azah Yusof. Carbon-based nanomaterials/allotropes: A glimpse of their synthesis, properties and some applications. *Materials*, 11(2):295, 2018.
- [3] Susmita Jana, Arka Bandyopadhyay, Sujoy Datta, Debaprem Bhat-tacharya, and Debnarayan Jana. Emerging properties of carbon based 2d material beyond graphene. *Journal of Physics: Condensed Matter*, 34(5):053001, 2021.
- [4] Xiong Zhang, Haitao Zhang, Chen Li, Kai Wang, Xianzhong Sun, and Yanwei Ma. Recent advances in porous graphene materials for supercapacitor applications. *Rsc Advances*, 4(86):45862–45884, 2014.
- [5] Xiaoyu Zheng, Jiayan Luo, Wei Lv, Da-Wei Wang, and Quan-Hong Yang. Two-dimensional porous carbon: synthesis and ion-transport properties. *Advanced Materials*, 27(36):5388–5395, 2015.
- [6] Mengcheng Wu, Wanying Zheng, Xi Hu, Feiyang Zhan, Qingqing He, Huayu Wang, Qichun Zhang, and Lingyun Chen. Exploring 2d energy storage materials: Advances in structure, synthesis, optimization strategies, and applications for monovalent and multivalent metal-ion hybrid capacitors. *Small*, 18(50):2205101, 2022.
- [7] Mingguang Wu, Jiaqin Liao, Lingxiao Yu, Ruitao Lv, Peng Li, Wenping Sun, Rou Tan, Xiaochuan Duan, Lei Zhang, Fang Li, et al. 2020 roadmap on carbon materials for energy storage and conversion. *Chemistry—An Asian Journal*, 15(7):995–1013, 2020.
- [8] Yuanyuan Zhang, Qijin Wan, and Nianjun Yang. Recent advances of porous graphene: synthesis, functionalization, and electrochemical applications. *Small*, 15(48):1903780, 2019.
- [9] Haibo Huang, Haodong Shi, Prateek Das, Jieqiong Qin, Yaguang Li, Xiao Wang, Feng Su, Pengchao Wen, Suyuan Li, Pengfei Lu, et al. The chemistry and promising applications of graphene and porous graphene materials. *Advanced Functional Materials*, 30(41):1909035, 2020.
- [10] PengTao Xu, JiXiang Yang, KeSai Wang, Zhen Zhou, and PanWen Shen. Porous graphene: Properties, preparation, and potential applications. *Chinese science bulletin*, 57:2948–2955, 2012.
- [11] Albert Guirguis, James W Maina, Xiwang Zhang, Luke C Henderson, Lingxue Kong, Hokyong Shon, and Ludovic F Dumée. Applications of nano-porous graphene materials—critical review on performance and challenges. *Materials Horizons*, 7(5):1218–1245, 2020.
- [12] Ding Zhou, Yi Cui, Pei-Wen Xiao, Mei-Yang Jiang, and Bao-Hang Han. A general and scalable synthesis approach to porous graphene. *Nature communications*, 5(1):4716, 2014.
- [13] Ali E Aliev, Yongzhe Guo, Alexandre F Fonseca, Joselito M Razal, Zhong Wang, Douglas S Galvão, Claire M Bolding, Nathaniel E Chapman-Wilson, Victor G Desyatkin, Johannes E Leisen, et al. A planar-sheet nongraphitic zero-bandgap sp² carbon phase made by the low-temperature reaction of γ -graphyne. *Proceedings of the National Academy of Sciences*, 122(5):e2413194122, 2025.
- [14] Victor G Desyatkin, William B Martin, Ali E Aliev, Nathaniel E Chapman, Alexandre F Fonseca, Douglas S Galvão, Ericka Roy Miller, Kevin H Stone, Zhong Wang, Dante Zakhidov, et al. Scalable synthesis and characterization of multilayer γ -graphyne, new carbon crystals with a small direct band gap. *Journal of the American Chemical Society*, 144(39):17999–18008, 2022.
- [15] Yan Fang, Yuxin Liu, Lu Qi, Yurui Xue, and Yuliang Li. 2d graphdiyne: an emerging carbon material. *Chemical Society Reviews*, 51(7):2681–2709, 2022.
- [16] Alexandre Cavalheiro Dias, Carlos Derli Almeida Cornelio, Mauricio Jeomar Piotrowski, Luiz Antonio Ribeiro Junior, Carlos Maciel de Oliveira Bastos, Celso Ricardo Caldeira Reego, and Diego Guedes-Sobrinho. Can 2d carbon allotropes be used as photovoltaic absorbers in solar harvesting devices? *ACS Applied Energy Materials*, 7(19):8572–8582, 2024.
- [17] Boris I Kharisov, Oxana V Kharissova, Lucy T González, Yolanda Peña Méndez, Igor E Uflyand, and Naveen Kulkarni. Density function theory predicted carbon allotropes: Recent developments. *Chemistry-Select*, 8(24):e202301567, 2023.
- [18] Xin Gao, Huibiao Liu, Dan Wang, and Jin Zhang. Graphdiyne: synthesis, properties, and applications. *Chemical Society Reviews*, 48(3):908–936, 2019.
- [19] Qitang Fan, Linghao Yan, Matthias W Tripp, Ondřej Krejčí, Stavrina Dimosthenous, Stefan R Kachel, Mengyi Chen, Adam S Foster, Ulrich Koert, Peter Liljeroth, et al. Biphenylene network: A nonbenzenoid carbon allotrope. *Science*, 372(6544):852–856, 2021.
- [20] Yu Liu, Gang Wang, Qingsong Huang, Liwei Guo, and Xiaolong Chen. Structural and electronic properties of t graphene: A two-dimensional carbon allotrope with tetrarings. *Physical review letters*, 108(22):225505, 2012.
- [21] Shunhong Zhang, Jian Zhou, Qian Wang, Xiaoshuang Chen, Yoshiyuki Kawazoe, and Puru Jena. Penta-graphene: A new carbon allotrope. *Proceedings of the National Academy of Sciences*, 112(8):2372–2377, 2015.
- [22] Raphael M Tromer, Marcelo L Pereira Junior, Kleuton A L. Lima, Alexandre F Fonseca, Luciano R da Silva, Douglas S Galvão, and Luiz A Ribeiro Junior. Mechanical, electronic, and optical properties of 8-16-4 graphyne: A 2d carbon allotrope with dirac cones. *The Journal of Physical Chemistry C*, 127(25):12226–12234, 2023.
- [23] ML Pereira Júnior, Wiliam Ferreira da Cunha, William Ferreira Giozza, Rafael Timoteo de Sousa Junior, and LA Ribeiro Junior. Irida-graphene: A new 2d carbon allotrope. *FlatChem*, 37:100469, 2023.
- [24] Roya Majidi. Irida-graphyne: A promising material for optoelectronic applications. *Materials Today Communications*, 38:107641, 2024.
- [25] Kleuton AL Lima, Rodrigo AF Alves, Daniel A da Silva, Fábio LL Mendonça, Marcelo L Pereira, and Luiz A Ribeiro. Th-graphyne: a new porous bidimensional carbon allotrope. *Physical Chemistry Chemical Physics*, 2025.
- [26] KAL Lima, Fábio Ferreira Monteiro, EJA Santos, RAF Alves, William Ferreira Giozza, and LA Ribeiro Junior. Dodecanophene: A novel 2d carbon allotrope with untunable metallic behavior under stress. *Materials Today Communications*, 40:109455, 2024.
- [27] Qi Song, Bing Wang, Ke Deng, Xinliang Feng, Manfred Wagner, Julian D Gale, Klaus Müllen, and Linjie Zhi. Graphenylene, a unique two-dimensional carbon network with nondelocalized cyclohexatriene units. *Journal of Materials Chemistry C*, 1(1):38–41, 2013.

- [28] José AS Laranjeira, Nicolas F Martins, Pablo A Denis, and Julio R Sambrano. Graphenyldiene: A new sp²-graphene-like nanosheet. *Carbon Trends*, 14:100321, 2024.
- [29] Christopher P Ewels, Xavier Rocquefelte, Harold W Kroto, Mark J Rayson, Patrick R Briddon, and Malcolm I Heggie. Predicting experimentally stable allotropes: Instability of penta-graphene. *Proceedings of the National Academy of Sciences*, 112(51):15609–15612, 2015.
- [30] Anubhav Jain, Yongwoo Shin, and Kristin A Persson. Computational predictions of energy materials using density functional theory. *Nature Reviews Materials*, 1(1):1–13, 2016.
- [31] Rampi Ramprasad, Rohit Batra, Ghanshyam Pilania, Arun Mannodi-Kanakkithodi, and Chiho Kim. Machine learning in materials informatics: recent applications and prospects. *npj Computational Materials*, 3(1):54, 2017.
- [32] Maria Lúcia Álvares Paz, Aldilene Saraiva-Souza, Vincent Meunier, and Eduardo Costa Girão. Naphthylenes: 1d and 2d carbon allotropes based on naphthyl units. *Carbon*, 153:792–803, 2019.
- [33] Harold Hart and Akira Oku. Synthesis and chemistry of octamethylnaphthalene. *Journal of Organic Chemistry*, 37(26):4269–4274, 1972.
- [34] Dong Han and Junfa Zhu. Surface-assisted fabrication of low-dimensional carbon-based nanoarchitectures. *Journal of Physics: Condensed Matter*, 33(34):343001, 2021.
- [35] Katsuhiko Ariga. Materials nanoarchitectonics: collaboration between chem, nano and mat. *ChemNanoMat*, 9(7):e202300120, 2023.
- [36] Sylvain Clair and Dimas G de Oteyza. Controlling a chemical coupling reaction on a surface: tools and strategies for on-surface synthesis. *Chemical reviews*, 119(7):4717–4776, 2019.
- [37] Pierre Hohenberg and Walter Kohn. Inhomogeneous electron gas. *Physical review*, 136(3B):B864, 1964.
- [38] Georg Kresse and Daniel Joubert. From ultrasoft pseudopotentials to the projector augmented-wave method. *Physical review b*, 59(3):1758, 1999.
- [39] John P Perdew, Kieron Burke, and Matthias Ernzerhof. Generalized gradient approximation made simple. *Physical review letters*, 77(18):3865, 1996.
- [40] Georg Kresse and Jürgen Furthmüller. Efficient iterative schemes for ab initio total-energy calculations using a plane-wave basis set. *Physical review B*, 54(16):11169, 1996.
- [41] Stefan Grimme. Semiempirical gga-type density functional constructed with a long-range dispersion correction. *Journal of computational chemistry*, 27(15):1787–1799, 2006.
- [42] Atsushi Togo and Isao Tanaka. First principles phonon calculations in materials science. *Scripta Materialia*, 108:1–5, 2015.
- [43] Shuichi Nosé. A unified formulation of the constant temperature molecular dynamics methods. *The Journal of chemical physics*, 81(1):511–519, 1984.
- [44] William G Hoover. Canonical dynamics: Equilibrium phase-space distributions. *Physical review A*, 31(3):1695, 1985.
- [45] Elaine A Moore and Lesley E Smart. Optical properties of solids. In *Solid State Chemistry*, pages 283–314. CRC Press, 2020.
- [46] Mauro Ferrero, Michel Rérat, Roberto Orlando, and Roberto Dovesi. Coupled perturbed hartree-fock for periodic systems: The role of symmetry and related computational aspects. *The Journal of chemical physics*, 128(1), 2008.
- [47] Roberto Dovesi, Roberto Orlando, Bartolomeo Civalleri, Carla Roetti, Victor R Saunders, and Claudio M Zicovich-Wilson. Crystal: a computational tool for the ab initio study of the electronic properties of crystals. *Zeitschrift für Kristallographie-Crystalline Materials*, 220(5-6):571–573, 2005.
- [48] Daniel Vilela Oliveira, Joachim Laun, Michael F Peintinger, and Thomas Bredow. Bsse-correction scheme for consistent gaussian basis sets of double-and triple-zeta valence with polarization quality for solid-state calculations. *Journal of Computational Chemistry*, 40(27):2364–2376, 2019.
- [49] Xian-Lei Sheng, Qing-Bo Yan, Fei Ye, Qing-Rong Zheng, and Gang Su. T-carbon: a novel carbon allotrope. *Physical review letters*, 106(15):155703, 2011.
- [50] Jin-Wu Jiang, Jiantao Leng, Jianxin Li, Zhengrong Guo, Tienchong Chang, Xingming Guo, and Tongyi Zhang. Twin graphene: A novel two-dimensional semiconducting carbon allotrope. *Carbon*, 118:370–375, 2017.
- [51] Li Zeng, Yingxiang Cai, Zhihao Xiang, Yu Zhang, and Xuechun Xu. A new metallic π -conjugated carbon sheet used for the cathode of li–s batteries. *RSC advances*, 9(1):92–98, 2019.
- [52] Nobuo Narita, Sumiaki Nagai, Shugo Suzuki, and Kenji Nakao. Optimized geometries and electronic structures of graphyne and its family. *Physical Review B*, 58(16):11009, 1998.
- [53] Qi-Shi Du, Pei-Duo Tang, Hua-Lin Huang, Fang-Li Du, Kai Huang, Neng-Zhong Xie, Si-Yu Long, Yan-Ming Li, Jie-Shan Qiu, and Ri-Bo Huang. A new type of two-dimensional carbon crystal prepared from 1, 3, 5-trihydroxybenzene. *Scientific reports*, 7(1):40796, 2017.
- [54] Andre K Geim and Konstantin S Novoselov. The rise of graphene. *Nature materials*, 6(3):183–191, 2007.
- [55] Trevor Jenkins, Alexander Martins Silva, Marcos G Menezes, Timo Thonhauser, and Saif Ullah. Thd-c sheet: A novel nonbenzenoid carbon allotrope with tetra-, hexa-, and dodeca-membered rings. *The Journal of Physical Chemistry C*, 128(26):10982–10996, 2024.
- [56] Vincent J Esposito, Louis J Allamandola, Christiaan Boersma, Jesse D Bregman, Ryan C Fortenberry, Alexandros Maragkoudakis, and Pasquale Temi. Anharmonic ir absorption spectra of the prototypical interstellar pahn phenanthrene, pyrene, and pentacene in their neutral and cation states. *Molecular Physics*, 122(7-8):e2252936, 2024.
- [57] Sergey M Kuznetsov, Elena A Sagitova, Kirill A Prokhorov, Dmitry I Mendeleev, Gulnara Yu Nikolaeva, Leila Yu Ustynuk, Arnulf Materny, and Patrice Donfack. Dependence of cc stretching wavenumber on polyene length in degraded polyvinyl chloride: a comparative empirical, classical mechanics, and dft study. *Spectrochimica Acta Part A: Molecular and Biomolecular Spectroscopy*, 282:121653, 2022.
- [58] Max Born. On the stability of crystal lattices. i. In *Mathematical Proceedings of the Cambridge Philosophical Society*, volume 36, pages 160–172. Cambridge University Press, 1940.